Thermodynamic Analysis of Ocean Circulation

J. NYCANDER, J. NILSSON, K. DÖÖS, AND G. BROSTRÖM

Department of Meteorology, Stockholm University, Stockholm, Sweden

(Manuscript received 11 January 2006, in final form 11 December 2006)

ABSTRACT

Calculating a streamfunction as function of depth and density is proposed as a new way of analyzing the thermodynamic character of the overturning circulation in the global ocean. The sign of an overturning cell in this streamfunction directly shows whether it is driven mechanically by large-scale wind stress or thermally by heat conduction and small-scale mixing. It is also shown that the integral of this streamfunction gives the thermodynamic work performed by the fluid. The analysis is also valid for the Boussinesq equations, although formally there is no thermodynamic work in an incompressible fluid. The proposed method is applied both to an idealized coarse-resolution three-dimensional numerical ocean model, and to the realistic high-resolution Ocean Circulation and Climate Advanced Model (OCCAM). It is shown that the overturning circulation in OCCAM between the 200- and 1000-m depth is dominated by a thermally indirect cell of 24 Sverdrups (1 Sv $\equiv 10^6$ m^3 s^{-1}), forced by Ekman pumping. In the densest and deepest waters there is a thermally direct cell of 18 Sv, which requires a forcing by around 100 GW of parameterized small-scale mixing.

1. Introduction

Is the ocean circulation thermally or mechanically forced? Already a century ago, Sandström (1908) concluded from his laboratory experiments that the heating and cooling at the ocean surface by itself would not be able to excite a circulation in the interior of the ocean. His arguments were elaborated by Jeffreys (1925) and Defant (1961), who concluded that the circulation must be mechanically forced. Nevertheless, for a long time, a widespread view among oceanographers was that a significant part of the ocean circulation (the thermohaline circulation) is forced by buoyancy fluxes at the surface (most importantly by the differential heating).

During the last decade this issue has been discussed intensively in the oceanographic literature (Munk and Wunsch 1998; Huang 1999; Paparella and Young 2002; Wunsch and Ferrari 2004; Mullarney et al. 2004; Gade and Gustafsson 2004; Marchal 2007). We will not try to recapitulate this discussion here, but merely point out that it has, in our opinion, suffered from a lack of adequate analysis tools.

A common way of analyzing the energetics of the ocean circulation is to perform bulk calculations and construct box diagrams (Munk and Wunsch 1998; Wunsch and Ferrari 2004). Such a diagram can be regarded as a zero-dimensional picture of the ocean, with no spatial degrees of freedom. For example, the global tidal forcing is represented by just one number. However, the same amount of mechanical or thermal forcing has different effects if it is applied at several thousand meters depth or at the surface.

There have also been some applications of one-dimensional models. One example is the idealized tube model of the overturning circulation proposed by Huang (1999). Another one is the thermodynamic analysis by Gade and Gustafsson (2004). They plotted a hypothetical closed particle trajectory, meant to represent the overturning circulation, in a traditional thermodynamic pressure–volume (pV) diagram, using the correct equation of state and real data of the ocean stratification. A similar hypothetical closed circuit was used in the theoretical arguments by Defant (1961).

A principal problem with these one-dimensional models is that the particle trajectories in a three-dimensional fluid are in general not closed, even if the flow is exactly stationary and of a simple and idealized nature. Instead, the typical situation is that a single trajectory will eventually fill the whole fluid volume. This has been recognized for a long time in the field of nonlinear

Corresponding author address: J. Nycander, Dept. of Meteorology, Stockholm University, Stockholm S-106 91, Sweden.
E-mail: jonas@misu.su.se

DOI: 10.1175/JPO3113.1

dynamics (Lichtenberg and Lieberman 1983), and similar features were also seen in a recent study of the chaotic nature of particle trajectories in a three-dimensional ocean model (Nycander et al. 2002).

We here propose a novel way of analyzing the energetics and thermodynamics of the ocean circulation: by computing the streamfunction in depth–density coordinates. This can be done by computing the vertical transport across levels of constant depth between curves of constant density. Alternatively, it can be done by computing the transport across surfaces of constant density between levels of constant depth. Since depth is linearly related to pressure by the hydrostatic relation, and density is just the inverse of specific volume, this streamfunction in effect displays the global overturning circulation in a traditional pV diagram, with immediate thermodynamic interpretation. For example, the sign of the various overturning cells directly shows whether they are thermally or mechanically forced. (Note that if small-scale mixing is parameterized as diffusion, a cell that is forced by this mixing appears as thermally forced in the model.)

Thus, the streamfunction in depth–density coordinates gives a two-dimensional thermodynamic picture of the ocean circulation, without any assumption about closed particle trajectories. However, for the definition of this streamfunction to be consistent, the circulation must be stationary, at least in a statistical sense.

There are several other ways of displaying the overturning circulation in a two-dimensional diagram. The most common one is to plot the overturning streamfunction in depth–latitude coordinates. This is straightforward to compute, and shows the zonally averaged velocity field. However, this average reveals little of the structure of the underlying three-dimensional field, and may give a very false impression of the movement of the various water masses. A notable example of this is the Deacon cell in the Southern Ocean (Döös and Webb 1994).

One way of improving the representation of the Lagrangian transport is to compute the residual streamfunction defined in the transformed Eulerian mean (TEM) theory (Andrews and McIntyre 1976; Karsten et al. 2002). A correction term is then added to the traditional streamfunction, in order to account for eddy transport. (The latter may be caused by either transient eddies, i.e., time-dependent fluctuations, or to standing eddies, i.e., longitude-dependent features in the flow field.) Another way of achieving a similar goal is to display the particle trajectories on a Poincaré section (Nycander et al. 2002).

In general, ocean currents tend to follow isopycnal surfaces, rather than surfaces of constant depth. With this in mind, the streamfunction has been computed in density–latitude coordinates instead of depth–latitude coordinates (Döös and Webb 1994). Essentially, this means that the velocity is averaged along curves of constant potential density, instead of constant depth. This streamfunction gives a better picture of the water mass movement than the traditional one. It also singles out the cross-isopycnal velocity component, the one that directly involves water mass transformation. (When using depth–latitude coordinates, on the other hand, the vertical velocity component may be dominated by adiabatic flow along sloping isopycnal surfaces.)

The streamfunction in depth–density coordinates was recently studied by Nurser and Lee (2004a,b). They proposed it as an alternative to using density–latitude coordinates, and investigated its relation to the TEM theory. One argument for using depth as a coordinate instead of latitude is that it is physically more important. In particular, the ocean surface is of central importance, but this surface does not have a specific location in plot with density and latitude as coordinates. However, the thermodynamic implications, which we believe are the main advantage of using depth and density as coordinates, were not mentioned by Nurser and Lee.

In the present paper, we will first show that the integral of the streamfunction in depth–density coordinates gives the total thermodynamic work performed by the fluid. It will also be shown that this conclusion holds even when the Boussinesq approximation is done, although the thermodynamic work formally vanishes in an incompressible fluid. We will then demonstrate the usefulness of the proposed method by calculating the streamfunction in depth–density coordinates for two different three-dimensional circulation models: a simple and idealized model, and the realistic high-resolution global Ocean Circulation and Climate Advanced Model (OCCAM).

2. Work done by thermal forces

In the present section we define the streamfunction in depth–density coordinates, and show that the integral of this streamfunction gives the total work performed by the fluid. We also show that if the relative density variation is small, this work is the same as the conversion of potential energy to kinetic energy. The analysis is very general, since it uses only universal kinematic relations and the equation of continuity, and does not require the momentum equation or the equation of state to be specified.

We start from the classical thermodynamic expression for the work W performed by some enclosed homogeneous fluid undergoing cyclic thermodynamic changes:

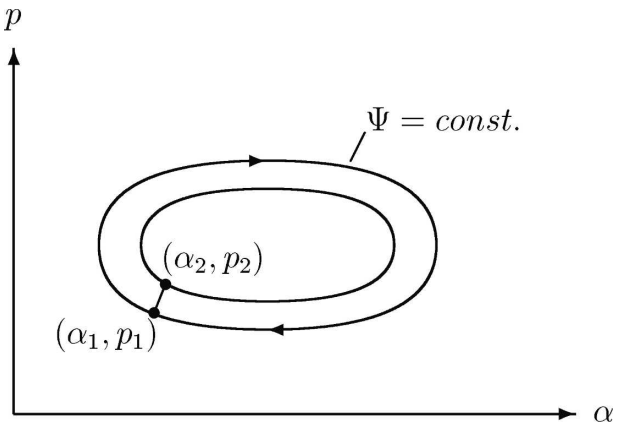

FIG. 1. Sketch of the streamfunction Ψ with the specific volume α and the pressure p as coordinates.

$$W = \oint p\, dV. \tag{1}$$

Here p is the pressure and V is the volume of the enclosed fluid.

We now generalize this to an inhomogeneous three-dimensional flow. Assume that the circulation is stationary, in the sense that the temperature, salinity, and density fields are stationary. It is not necessary that individual fluid particles undergo cyclical motion. It is then possible to define a streamfunction Ψ with the pressure p and the specific volume $\alpha = 1/\rho$ as coordinates (cf. Fig. 1). We define the difference $\Psi(\alpha_2, p_2) - \Psi(\alpha_1, p_1)$ as the mass flux (kg s^{-1}) across the surface bounded by the two fluid curves defined by (α_1, p_1) and (α_2, p_2). This may, for example, be the vertical flux across a surface of constant depth ($\approx$constant pressure) between two isotherms.

Note that if the flow is nonstationary, this streamfunction cannot be consistently defined. This is because the net mass flux across any closed curve in the $p\alpha$ diagram given by such a streamfunction vanishes identically. Consider, for example, a situation in which the fluid is warming up. In this case there is a net mass flux into regions of the $p\alpha$ diagram with comparatively low density; such a flux cannot be described by a streamfunction.

Now consider two closed streamlines in the $p\alpha$ diagram, one just inside the other, as in Fig. 1, with the mass flux $d\Psi$ between them. During the time δt the mass $\delta m = \delta t d\Psi$ flows past any line connecting the two streamlines in the $p\alpha$ diagram. The additive effect of the displacements of all fluid parcels between these two streamlines during this time is the same as if the mass δm alone had made a full circuit. The volume change dV of this mass during a small part of this circuit is

$$dV = \delta m d\alpha. \tag{2}$$

Hence, the work done by all the fluid between the two streamlines during the time δt is

$$\delta W = \oint p\, dV = \oint p \delta m\, d\alpha = \oint p \delta t\, d\Psi\, d\alpha.$$

Hence,

$$\frac{dW}{dt} = d\Psi \oint p\, d\alpha.$$

Let us denote the total amount of work done by all the fluid per unit time by M. This is obtained by integrating the previous expression over all values of Ψ:

$$M = \int d\Psi \oint p\, d\alpha. \tag{3}$$

This integral can be thought of as the volume under the surface defined by $\Psi(\alpha, p)$ in Fig. 1.

Equation (3) is the desired result. However, in order to demonstrate the equivalence between this equation and more familiar expressions, we now rewrite M as an integral in the usual Eulerian coordinates. Integrating by parts with respect to α, and noting that the mass flux across a surface element $d\mathbf{S}$ is $d\Psi = \rho \mathbf{v} \cdot d\mathbf{S}$, where $\rho = 1/\alpha$, we obtain

$$M = -\int\int \mathbf{v} \cdot d\mathbf{S}\, dp.$$

Let $\hat{\mathbf{p}}$ be the unit vector perpendicular to surfaces $p =$ constant, so that $d\mathbf{S} = \hat{\mathbf{p}} dS$, and let l be a length coordinate in the same direction (essentially a vertical coordinate). Then,

$$d\mathbf{S}dp = dS\hat{\mathbf{p}}dp = dS\nabla p dl = \nabla p dV.$$

Note that here and below, dV is a conventional Eulerian volume element, and not the volume change of a particular fluid mass, as in Eqs. (1)–(2) above. We obtain

$$M = -\int \mathbf{v} \cdot \nabla p\, dV, \tag{4}$$

where the integral is taken over the whole fluid volume. Integrating by parts, and assuming that either the normal velocity component (at the bottom of the ocean) or the pressure (at the surface) vanish at the boundaries, we obtain

$$M = \int p \nabla \cdot \mathbf{v}\, dV. \tag{5}$$

From the continuity equation we have

$$\nabla \cdot \mathbf{v} = \rho \frac{d\alpha}{dt}.$$

Equation (5) can then be written

$$M = \int p \frac{d\alpha}{dt} \rho \, dV = \int p \frac{d\alpha}{dt} dm. \tag{6}$$

Equation (6) can also be obtained directly by noting that $(p)d\alpha/dt$ is the rate of work performed by a fluid per unit mass, in agreement with Eq. (1).

So far we have assumed that the density and pressure fields are stationary. However, Eq. (6) defines the work performed by pressure forces even for a time-dependent flow, and this is still equivalent to Eqs. (4) or (5), which do not contain Ψ.

We now consider a time-dependent flow, and assume that the relative changes of density are small:

$$\alpha = \alpha_0 + \alpha_1 \quad \text{and}$$
$$\rho = \rho_0 + \rho_1,$$

where $\rho_1/\rho_0 \sim \alpha_1/\alpha_0 \ll 1$ and ρ_0 and α_0 are constant. We have

$$\alpha_0 = \frac{1}{\rho_0} \quad \text{and}$$
$$\alpha_1 \simeq -\alpha_0^2 \rho_1. \tag{7}$$

We also assume that the pressure is hydrostatic:

$$\frac{\partial p}{\partial z} = -g\rho. \tag{8}$$

Rewrite Eq. (6) using these approximations:

$$M = \int p \frac{d\alpha_1}{dt} \rho \, dV \simeq -\int \rho_0^2 gz \frac{d\alpha_1}{dt} dV \simeq \int gz \frac{d\rho_1}{dt} dV$$
$$= \int gz \left(\frac{\partial \rho_1}{\partial t} + \mathbf{v} \cdot \nabla \rho_1 \right) dV. \tag{9}$$

The assumption of small relative density changes implies that $\nabla \cdot \mathbf{v}$ is small, so that $\nabla \cdot (z\mathbf{v}) \simeq w$, where w is the vertical velocity component. Integrating the second term of Eq. (9) by parts we therefore get:

$$M \simeq \frac{dU}{dt} + C, \tag{10}$$

where the potential energy is defined by

$$U = \int gz\rho_1 \, dV, \tag{11}$$

and C is the conversion rate from potential energy to kinetic energy,

$$C = -\int gw\rho_1 \, dV. \tag{12}$$

Thus, we have shown that if the circulation is stationary (i.e., $dU/dt = 0$), and the relative density variation is small, the total thermodynamic work done by the fluid is the same as the conversion from potential to kinetic energy.

3. Energetics of the Boussinesq equations

Very often the Boussinesq equations are used for ocean modeling. However, since they assume the flow to be incompressible, it may appear that they are unable to describe thermodynamic work. The present section is devoted to an analysis of the energetics of these equations, in order to clarify how the thermodynamic work can in fact be diagnosed from them.

The Boussinesq equations with a linear equation of state are

$$\rho_0 \left(\frac{\partial \mathbf{v}}{\partial t} + \mathbf{v} \cdot \nabla \mathbf{v} + f\hat{\mathbf{z}} \times \mathbf{v} \right) = -\nabla p - \hat{\mathbf{z}} g \rho_1 + \mu \nabla^2 \mathbf{v}, \tag{13}$$

$$\nabla \cdot \mathbf{v} = 0 \quad \text{and} \tag{14}$$

$$\frac{\partial \rho_1}{\partial t} = -\nabla \cdot (\mathbf{v}\rho_1 + \mathbf{b}). \tag{15}$$

Here $\hat{\mathbf{z}}$ is the vertical unit vector, μ is the dynamic viscosity, p is the pressure perturbation, and $\mathbf{b}$ is the nonadvective density flux, which may include conduction and radiation of heat, molecular diffusion, and parameterized turbulent transports (e.g., convection). (Note that in numerical modeling, different values are often assigned to the horizontal and the vertical eddy viscosities. For simplicity, however, we here assume the viscosity to be isotropic.) To derive the equation for kinetic energy, we multiply Eq. (13) by $\mathbf{v} \cdot$ and integrate over the total fluid volume. Using the boundary condition $\mathbf{v} \cdot d\mathbf{S} = 0$ we obtain

$$\frac{d}{dt} \int \rho_0 \frac{|\mathbf{v}|^2}{2} dV = -\int gw\rho_1 \, dV + \mu \int \mathbf{v} \cdot \nabla^2 \mathbf{v} \, dV. \tag{16}$$

Integrating the last term in Eq. (16) by parts gives

$$\mu \int v_i \nabla^2 v_i \, dV = -\mu \int \nabla v_i \cdot \nabla v_i \, dV + \mu \oint v_i \nabla v_i \cdot d\mathbf{S},$$

where v_i represents the three velocity components, and summation over repeated indices is understood. The first term on the right-hand side is the rate of viscous dissipation:

$$D = \mu \int \|\nabla \mathbf{v}\|^2 \, dV. \tag{17}$$

Here, D is positive definite. In the second term we identify the surface stress,

$$\boldsymbol{\tau} = \mu(\hat{\mathbf{n}} \cdot \nabla)\mathbf{v},$$

where $\hat{\mathbf{n}}$ is the unit vector normal to the boundary, $d\mathbf{S} = \hat{\mathbf{n}}ds$. This term can then be written as

$$T = \oint \mathbf{v} \cdot \boldsymbol{\tau}\, dS, \tag{18}$$

which is the generation of kinetic energy by surface stress (e.g., wind stress). In the case of a rigid boundary with a no-slip condition we have $T = 0$, and the bottom stress therefore does not affect the energy budget directly.

Identifying the kinetic energy,

$$K = \int \rho_0 \frac{|\mathbf{v}|^2}{2}\, dV, \tag{19}$$

and the conversion rate C from potential energy to kinetic energy from Eq. (12), Eq. (16) can now be written as

$$\frac{dK}{dt} = C + T - D. \tag{20}$$

To derive the corresponding equation for potential energy, we multiply Eq. (15) by gz and integrate over the total fluid volume. Integrating by parts we obtain

$$\frac{d}{dt}\int g\rho_1 z\, dV = \int gw\rho_1\, dV + g\int \hat{\mathbf{z}} \cdot \mathbf{b}\, dV - g\oint z\mathbf{b} \cdot d\mathbf{S}. \tag{21}$$

On the left-hand side we here identify the potential energy from Eq. (11). Define

$$P_i = g\int \hat{\mathbf{z}} \cdot \mathbf{b}\, dV \quad \text{and} \tag{22}$$

$$P_b = -g\oint z\mathbf{b} \cdot d\mathbf{S}. \tag{23}$$

Here, P_i is the potential energy created by the nonadvective density flux in the interior of the fluid. It is positive if this flux is upward (corresponding to downward heat flux), so that it raises the center of mass. If the nonadvective density flux is diffusive, we have

$$\hat{\mathbf{z}} \cdot \mathbf{b} = -\kappa \frac{\partial \rho_1}{\partial z},$$

where κ is the vertical diffusivity. If the fluid is stably stratified (i.e., $\partial\rho_1/\partial z < 0$), then $P_i > 0$. Convection, on the other hand, is associated with upward heat flux and negative P_i.

The quantity P_b is the potential energy created by density fluxes across the boundaries. At points where $\mathbf{b} \cdot d\mathbf{S} < 0$, this flux tends to increase the density. This increases the potential energy if $z > 0$, and decreases it if $z < 0$. Note that we can choose any level as $z = 0$. A formal way to see this is to integrate Eq. (15) over the fluid volume, which gives

$$\frac{d}{dt}\int \rho_1\, dV = -\oint \mathbf{b} \cdot d\mathbf{S}.$$

It is easily seen that multiplying this equation by a constant coefficient and adding to Eq. (21) corresponds to shifting the level where $z = 0$.

Suppose that the heat flux into the fluid ($\nabla\rho_1 \cdot d\mathbf{S} < 0$) occurs at a higher level than the heat flux out of the fluid ($\nabla\rho_1 \cdot d\mathbf{S} > 0$). If we choose $z = 0$ to lie between these levels, we have $z\nabla\rho_1 \cdot d\mathbf{S} < 0$ everywhere, that is, $P_b < 0$. Thus, potential energy is in this case consumed at the boundaries, and the internal heat conduction is the only source of potential energy.

Another important case is when the heat flux is zero across all boundaries except the sea surface. Choosing $z = 0$ to be at the surface we then get $P_b = 0$.

Using Eqs. (12), (22), and (23), Eq. (21) can be written

$$\frac{dU}{dt} = -C + P_i + P_b. \tag{24}$$

To obtain the total energy budget we finally add Eqs. (20) and (24):

$$\frac{dE}{dt} = T - D + P_i + P_b, \tag{25}$$

where $E = K + U$ is the total energy.

In Fig. 2 we illustrate Eqs. (20) and (24) by a simple box diagram. We can imagine the following two typical scenarios for the ocean circulation, with $P_b = 0$. In the thermally direct case, $C > 0$, the only possible source of

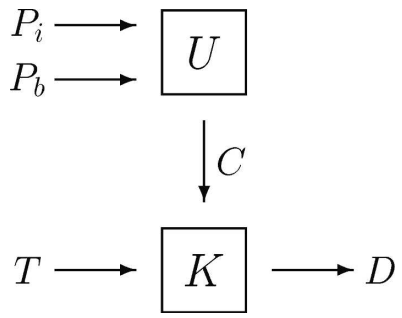

FIG. 2. Illustration of the budget equations [Eqs. (20) and (24)] for the kinetic energy K and the potential energy U in a Boussinesq model. The energy fluxes are defined as positive in the direction of the arrows. In reality, P_b is zero, T and D are positive, while P_i and C can have either sign.

potential energy is P_i, that is, heat conduction and small-scale mixing. Therefore, P_i must be positive. Kinetic energy is in this case supplied by conversion from potential energy, as well as by the wind stress T. In the thermally indirect case, $C < 0$, the only possible sink of potential energy is P_i, that is, convection, and wind stress is the only possible source of kinetic energy. The energy flux therefore begins with wind stress generating kinetic energy, which is partly dissipated directly and partly converted to potential energy, which is finally consumed by convection (i.e., in reality converted to small-scale, unresolved kinetic energy).

We now consider the work performed by thermal forces. This is in general given by Eq. (6), and it was shown in the previous section that this reduces to Eq. (10) when the relative density perturbation is small, as when using the Boussinesq approximation. If we compare Eq. (10) to the budget equation [Eq. (24)] for potential energy, we find

$$M = P_i + P_b. \tag{26}$$

Thus, although the pressure forces strictly speaking perform no work in a Boussinesq fluid, the thermodynamic work instead appears as the generation of potential energy by heat conduction.

If one wants to calculate the thermodynamic work in a simulation of the Boussinesq equations, it is possible to use Eq. (26). However, if the circulation is stationary, there is another possibility. In this case we obtain from Eqs. (10) and (12):

$$M = C = -\int g\rho_1 \mathbf{v} \cdot d\mathbf{S}\, dz,$$

where $d\mathbf{S} = \hat{\mathbf{z}} dx dy$. We introduce the streamfunction ψ for volume flux, which is related to the streamfunction Ψ for mass flux by

$$d\psi = \frac{d\Psi}{\rho_0}.$$

Setting $\mathbf{v} \cdot d\mathbf{S} = d\psi$ we obtain

$$M = \int gz\, d\psi\, d\rho_1 ,$$

where we integrated by parts. Since $gz = -p/\rho_0$ and $d\rho_1/\rho_0^2 = -d\alpha_1$, this is equivalent to Eq. (3). Integrating by parts once more, we finally obtain

$$M = -g\int \psi\, dz\, d\rho_1. \tag{27}$$

Thus, the thermodynamic work can be calculated as an integral of the streamfunction in a $z\rho_1$ diagram. An advantage of this method is that it makes it easy to see the contributions from different parts of the circulation, for example from different overturning cells.

We also note that integrating the streamfunction along a vertical or horizontal section in the density–depth diagram gives physically meaningful results. First integrate along the horizontal plane $z = z_c$:

$$-\int_{z=z_c} \psi\, d\rho_1 = \int_{z=z_c} \rho_1\, d\psi = \int_{z=z_c} \rho_1 w\, dS \equiv \Phi_\rho. \tag{28}$$

This is the advective part of the vertical density flux (buoyancy flux with reverse sign). Then integrate along an isopycnal surface $\rho_1 = \rho_c$:

$$-\int_{\rho_1=\rho_c} \psi\, dz = \int_{\rho_1=\rho_c} z\, d\psi = \int_{\rho_1=\rho_c} z\mathbf{v} \cdot d\mathbf{S}. \tag{29}$$

To interpret this we multiply Eq. (15) by gz and integrate over the volume enclosed by the isopycnal surface $\rho_1 = \rho_c$ and the sea surface. We obtain

$$\frac{dU}{dt} = -\rho_c g \int_{\rho_1=\rho_c} z\mathbf{v} \cdot d\mathbf{S} - C + P_b + P_i,$$

where U, C, P_i, and P_b are defined as in Eqs. (11), (12), (22), and (23), with the volume integrals taken over $\rho_1 < \rho_c$. We can thus define the advective flux Φ_U of potential energy across the isopycnal surface as

$$\Phi_U = \rho_c g \int_{\rho_1=\rho_c} z\mathbf{v} \cdot d\mathbf{S}.$$

Equation (29) may then be written

$$-\int_{\rho_1=\rho_c} \psi\, dz = \frac{\Phi_U}{\rho_c g}. \tag{30}$$

We end this section by considering the so-called Sandström's theorem (Sandström 1908). This theorem states that no circulation can be excited solely by heating and cooling the water surface (without mechanical forcing). This statement neglects the effect of heat conduction.

A rigorous formulation was given by Paparella and Young (2002). They considered statistically stationary solutions of Eqs. (13)–(15), with cooling and heating only at the surface, and no wind stress. Further, they considered the case in which the nonadvective buoyancy flux was purely diffusive. In this case $dE/dt = P_b = T = 0$, and Eq. (25) reduces to

$$D = P_i = -\kappa \int g \frac{\partial \rho_1}{\partial z}\, dV$$

$$= -\kappa g \int [\rho_1(0) - \rho_1(-H)]\, dx\, dy,$$

where H is the ocean depth. Dividing by the total fluid volume we obtain their central result (3.4), which provides a bound on the turbulent dissipation in terms of the molecular diffusivity κ.

Defant (1961) and Marchal (2007) considered the circulation around a closed circuit in a stationary flow. They found that in order to balance friction, the direction of the flow must be such that the thermodynamic work is positive; that is, fluid elements moving toward lighter (warmer) regions must be at higher pressures than those moving toward colder regions.

We can obtain a related statement for stationary flow described by the Boussinesq equations. From Eq. (10), we have $M = C$, and in the absence of wind forcing ($T = 0$), Eq. (20) gives

$$M = D \geq 0. \tag{31}$$

Thus, the circulation in a $z\rho_1$ diagram must on the average be positive, so that the thermodynamic work is positive. This result is valid even if there are no closed particle circuits, in contrast to the results obtained by Defant (1961) and Marchal (2007).

4. Analysis of an idealized model

We will now apply some of the concepts presented above to an idealized ocean circulation model. We have used the Massachusetts Institute of Technology general circulation model (MITgcm; Marshall et al. 1997a,b) to conduct simulations in a square basin with sloping boundaries. The model is hydrostatic and uses a linear equation of state. The basin is 6000 km $\times$ 6000 km, and its depth increases linearly from the coast to a maximum depth of 3000 m, which is reached 2000 km from the coast. The central part of the basin has a flat bottom.

The model uses Cartesian coordinates on an f plane, with $f = 10^{-4}\ \mathrm{s}^{-1}$. The horizontal grid spacing is 100 km and the grid has 60 $\times$ 60 points. The model has 25 vertical levels with a spacing ranging from 50 m at the surface to 200 m at the bottom. Horizontal and vertical viscosities are 5000 and $10^{-3}\ \mathrm{m}^2\ \mathrm{s}^{-1}$, respectively. The vertical diffusivity is $10^{-4}\ \mathrm{m}^2\ \mathrm{s}^{-1}$, while the horizontal mixing is represented by the Gent–McWilliams (GM) scheme with the isopycnal diffusivity $10^3\ \mathrm{m}^2\ \mathrm{s}^{-1}$. There is also a parameterized convection scheme that instantaneously removes any vertical instability by vertical mixing. The density depends linearly on temperature according to $\rho_1 = -\rho_0\alpha_T T$, where $\alpha_T = 2 \times 10^{-4}\ ^\circ\mathrm{C}^{-1}$. The boundary condition on the tangential velocity is no slip on the solid boundaries. At the surface, the temperature is restored toward the profile $\Delta T[\cos(\pi y/L) + 1]/2$, where $\Delta T = 20^\circ$C and L is the basin length. The restoring time scale is 12.5 days, implying that a deviation of 1°C from the restoring temperature yields a surface heat flux of 185 W m^{-2}. (Note that the thermal restoring is so rapid that the sea surface temperature is essentially prescribed.) A wind stress field, with the stress aligned with the x direction, is applied at the surface:

$$\tau_x = -\tau_0 \sin(2\pi y/L),$$

where τ_0 is the amplitude. This corresponds to easterly winds over the southern part of the basin and westerly winds over the northern part. The model is integrated for 2000 yr, which essentially allows the simulation to equilibrate with the thermal surface forcing (i.e., the model drift is negligible). At the end of the simulation, there are no time-dependent eddies in the model.

Figure 3 shows the temperature distribution in a y–z cross section in the midbasin, and the overturning circulation in the y–z plane, taken from simulations both without wind stress and with $\tau_0 = 0.05$ N m^{-2}. In both simulations, the horizontal flow is essentially in geostrophic balance and thus nondivergent. The dynamics and the structure of the horizontal flow in the case without wind forcing have been discussed in some detail by Nilsson et al. (2005). Here, we focus on the ageostrophic overturning circulation.

In the absence of wind forcing, the vertical motion occurs primarily within the bottom Ekman layer over the sloping boundaries. The overturning is shallow and essentially confined to the thermocline (see Fig. 3b). In essence, the overturning is associated with a northward flow near the surface, compensated by a southward flow at depth. Thus, the flow is thermally direct, with sinking in the cold part of the basin and upwelling in the warm part.

In the wind-forced case, the surface Ekman layer induces downwelling in the central basin and upwelling in the northern and southern parts of the basin. The vertical velocities at the base of the surface Ekman layer essentially penetrate to the bottom, which slightly deforms the temperature field and results in a deeper overturning circulation (see Figs. 3c,d). In the bulk of the northern part of the basin, where the wind forces a southward Ekman surface flow, the direction of the overturning is reversed. Nevertheless, the advective meridional heat flux, integrated vertically and across the basin, is still northward for all y (not shown).

We proceed to discuss the streamfunction in depth–density coordinates, which contains information on the energetics of the flow as discussed in section 2. Since the density depends linearly on temperature, we have here chosen to compute the streamfunction in z–T coordinates. We define the streamfunction $\psi(T, z)$ to rep-

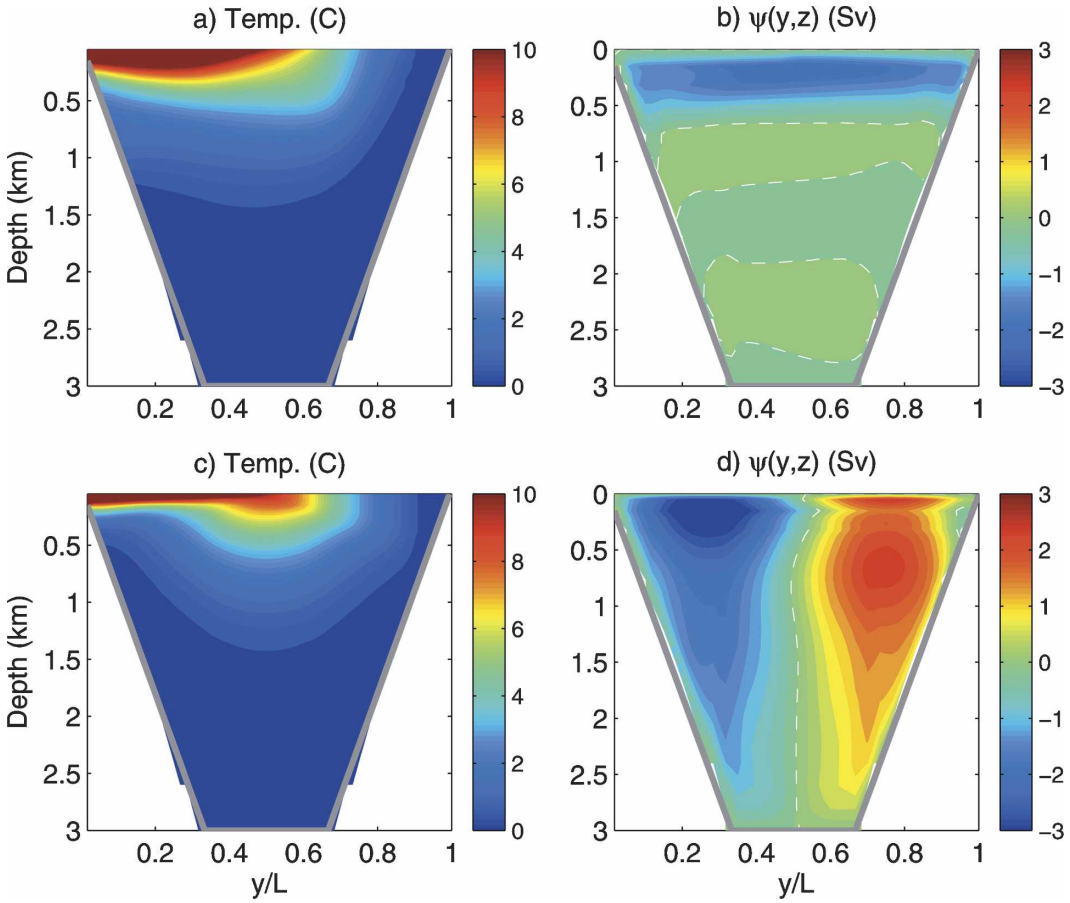

FIG. 3. (left) Temperature field and (right) overturning in the y–z plane from the idealized model simulations. In (a), (b), $\tau_0 = 0$ (no wind forcing) and in (c), (d), $\tau_0 = 0.05$ N m^{-2}. The transport is given in Sverdrups and is counted positive when the circulation is anticlockwise. The temperature field is taken from the midbasin and the bottom is indicated by the gray line.

resent the vertical volume transport at the level z of all water that is colder than T. Note that, as defined here, $\psi(T, z)$ is negative for thermally direct flow and positive for thermally indirect flow.

The nonadvective buoyancy flux in the model includes parameterized vertical transport due to small-scale turbulence, convection, and baroclinic eddies. These parameterized processes contribute to the generation or destruction of potential energy (i.e., P_i) in the model. In reality, they are associated with conversion between potential energy and kinetic energy at smaller scales than resolved in the model. This means that a circulation that is forced by unresolved small-scale mixing appears to be thermally forced (i.e., thermally direct) in the model. Conversely, a thermally indirect model circulation must be mechanically forced on the large resolved scales, that is, by the Ekman pumping caused by the wind stress.

The GM scheme parameterizes the effect of baroclinic eddies as a thickness diffusion that tends to relax the slope of the isopycnal surfaces. This is done by introducing a fictitious bolus velocity $\mathbf{v}^*$ (also called residual mean velocity). This velocity is added to the Eulerian velocity $\mathbf{v}$ in the density equation [Eq. (15)], but not in the momentum equation [Eq. (13)]. As a result, the potential energy in the model decreases, and this loss represents energy that is transferred to the unresolved eddies.

When we compute the streamfunction, we use only the Eulerian velocity. In this way we keep the property that the integral over the streamfunction equals the conversion C between potential and kinetic energy in the model. This corresponds to regarding the GM scheme simply as a sink of potential energy (similarly as the convection scheme). One could instead use the total velocity $\mathbf{v} + \mathbf{v}^*$, which would add an extra contribution to the streamfunction in the thermally driven direction. The integral over the streamfunction would then equal the conversion C plus the energy loss due to the GM scheme.

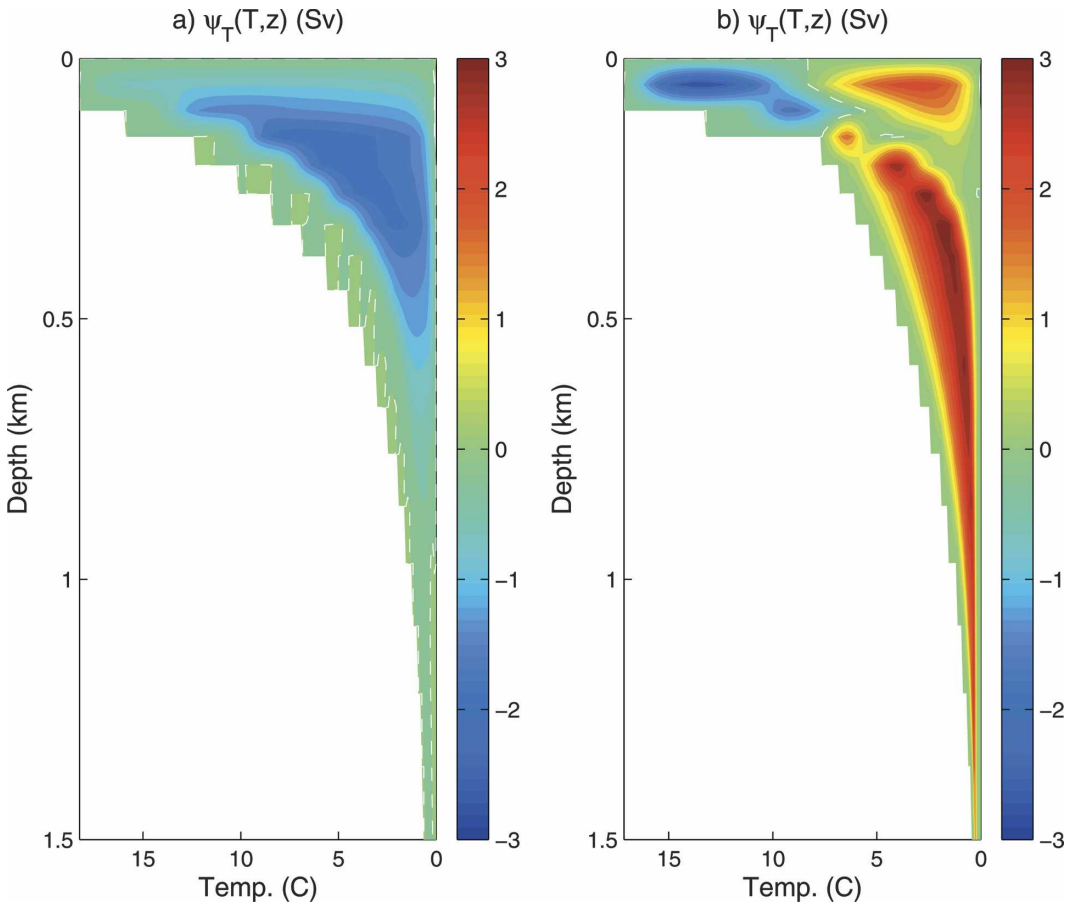

FIG. 4. Overturning streamfunction $\psi(T, z)$ (Sv) in depth–temperature coordinates from the idealized model for (a) $\tau_0 = 0$ and (b) $\tau_0 = 0.05$ N m^{-2}. Negative values of $\psi(T, z)$, corresponding to clockwise circulation, imply thermally direct circulation; i.e., the flow acts to lower the center of mass in that T–z range. Note that depths greater than 1.5 km, where $\psi(T, z)$ is small in the present simulations, have been omitted in the figure.

The streamfunctions computed by these two methods have different meaning, and comparing them would be helpful for understanding the energetic effects of the GM scheme. However, a detailed examination of this issue is outside the scope of the present article, and we have therefore chosen to display only the streamfunction computed from the Eulerian velocity.

The streamfunctions in z–T coordinates are shown in Fig. 4. In the case without wind forcing, the circulation consists of a single thermally direct cell. Thus, at a given depth, the warm fluid is rising whereas the cold fluid is sinking. Further, $\psi(T, z)$ shows that in the upper part of the basin the net flow across the isotherms is directed from warm to cold; in the deeper part of the basin the situation is reversed. The circulation is energetically sustained by the vertical mixing parameterized as diffusion, which creates potential energy by heating the fluid in the thermocline, that is, at higher pressure below the sea surface. This process is represented by P_i in Eq. (24). This creation of potential energy is balanced by the tendency of the overturning circulation to lower the center of mass. The released kinetic energy is lost by viscous dissipation.

In the presence of wind forcing, $\psi(T, z)$ also includes a thermally indirect cell, as seen in Fig. 4b. It occupies all of the deep ocean and extends to the surface for temperatures lower than about 5°. In the thermally indirect cell cold fluid is rising and warm fluid is sinking, which requires external mechanical forcing. The net near-surface flow in this cell is from cold to warm, which is associated with the southward flow in the Ekman layer in the northern part of the basin.

For stronger wind forcing, $\tau_0 = 0.1$ N m^{-2} and $\tau_0 = 0.2$ N m^{-2} (not shown), the thermally indirect circulation in the range of intermediate-to-cold temperatures becomes even more pronounced. In this case, the flow in the bulk of z–T space is mechanically forced. However, for high temperatures and close to the surface,

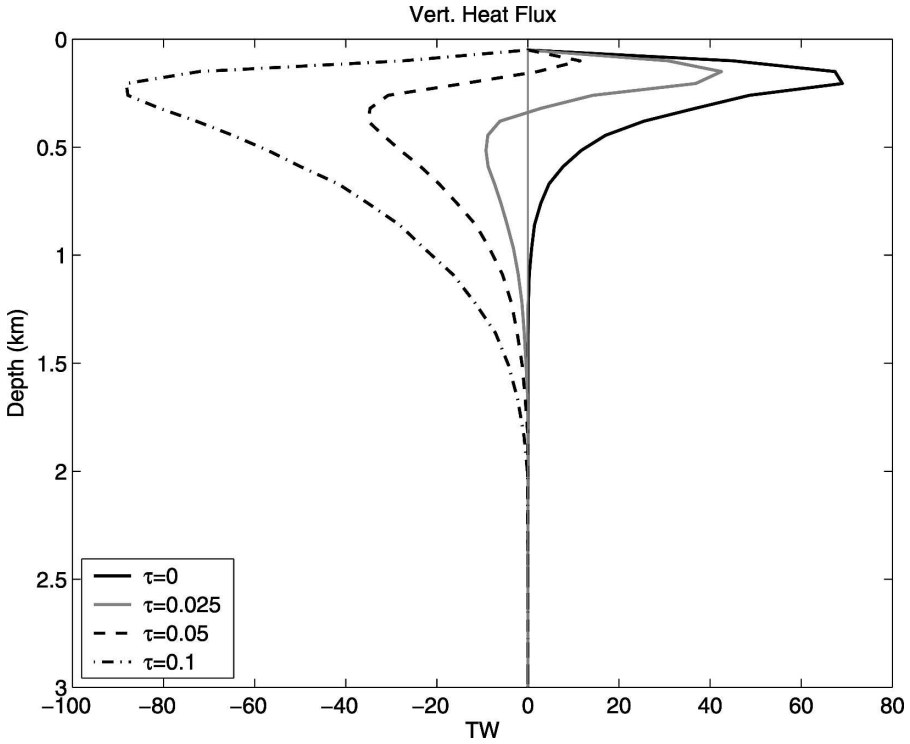

FIG. 5. Area-integrated vertical advective heat transport. Results for $\tau_0 = 0$ (solid line), $\tau_0 = 0.025$ N m^{-2} (gray line), $\tau_0 = 0.05$ N m^{-2} (dashed line), and $\tau_0 = 0.1$ N m^{-2} (dashed–dotted line) are shown.

there remains a thermally direct cell. It is remarkable that it is the deep circulation that becomes mechanically forced as the wind forcing increases, whereas the shallow circulation associated with the warmest water remains thermally direct. This feature is also seen in the diagnosis of the more realistic ocean model reported in the next section.

Next we consider the area-integrated vertical heat flux $\Phi_T(z)$ due to advection. This quantity is proportional to the vertical advective buoyancy flux and can according to Eq. (28) be calculated as

$$\Phi_T(z) = -c \int \psi(T, z)\, dT, \tag{32}$$

where the integral ranges over all temperatures and c is the heat capacity per unit volume. Figure 5 shows the vertical advective heat flux in simulations with different wind-forcing strengths. Without wind forcing, the flow transports heat upward over the entire range of depths. Essentially, this corresponds to the classical picture of a balance between upward advection and downward diffusion of heat (Munk 1966). When the wind forcing is increased, however, there is a tendency toward downward advection of heat. It is interesting to note that for weak wind forcing, the downward heat transport is confined to the deeper part of the basin whereas upward heat transport still occurs near the surface. For strong wind forcing, the flow transports heat downward at all depths.

The total conversion rate C from potential to kinetic energy in the different simulations is given in Table 1. It was obtained by integrating $(g\alpha_T\rho_0/c)\Phi_T(z)$ vertically, as seen from Eqs. (12) and (32). The results show that C becomes negative for stronger wind forcing, implying a thermally indirect circulation associated with a conversion from kinetic to potential energy. However, it is also seen from Table 1 that T_{wind} changes much more than C; that is, only a small part of the additional work performed by the surface wind stress is converted to potential energy. Thus, most of the additional work is lost by viscous dissipation (cf. Fig. 2).

The nonadvective vertical heat flux, which balances the advective flux, consists of three parts: a downward diffusive flux, an upward flux due to the parameterized convection, and a flux due to the GM scheme. The latter may be locally directed either upward or downward, but the horizontally integrated heat flux due to the GM scheme is always directed upward, that is, acting to decrease the potential energy. The rate of production of potential energy due to the three parts of the

TABLE 1. Rates of work per unit area (mW m^{-2}) computed from the idealized model for different amplitudes of the wind stress (τ_0) [see Eqs. (20) and (24)]. Here, T_{wind} is the rate of work performed by the surface wind stress, C is the conversion from potential to kinetic energy, and P_{diff}, P_{GM}, and P_{conv} are the production or destruction of potential energy due to vertical diffusion, the GM scheme, and parameterized convection, respectively. The convective contribution is diagnosed as a residual from the steady-state potential energy equation, i.e., $0 = -C + P_{diff} + P_{GM} + P_{conv}$.

τ_0 (N m^{-2})	T_{wind}	C	P_{diff}	P_{GM}	P_{conv}
0	0	0.26	1.78	−0.72	−0.80
0.025	0.45	0.03	1.81	−0.74	−1.04
0.05	1.59	−0.24	1.83	−0.74	−1.33
0.1	5.57	−0.70	1.86	−0.90	−1.67
0.2	19.66	−1.77	1.88	−1.39	−2.26

nonadvective vertical heat flux is given in Table 1. We note that even in the purely thermally driven case (without wind stress), most of the potential energy created by the diffusive vertical mixing is consumed by the convection and GM schemes, rather than converted to kinetic energy. In the upper 200 m of the model, the diffusive and the convective fluxes nearly balance each other and are significantly greater than the fluxes because of the advection and the GM scheme. At deeper levels, the diffusive downward flux remains significant, whereas the GM scheme provides the dominating upward heat flux; the advective flux is of importance only in the strongly wind-forced cases.

Note that much of the information about the conversion from potential to kinetic energy that is contained in the two-dimensional field $\psi(T, z)$ is lost in the integrated quantities $\Phi_T(z)$ and C. In the simulation with $\tau_0 = 0.1$ N m^{-2}, for instance, $\Phi_T(z)$ is negative for all depths, indicating a thermally indirect flow. However, the streamfunction $\psi(T, z)$ (not shown) reveals the presence of a thermally direct cell in the warmest waters near the surface.

5. Results from a realistic general circulation model

In the present section we will apply the proposed analysis method to the eddy resolving general circulation model OCCAM. This model has the horizontal resolution 1/4° at the equator and 66 depth levels, and is forced with realistic six-hourly atmospheric fields (except for precipitation, cloudiness and shortwave radiation, where monthly fields were used). It has a parameterized convection scheme similar to the one in the MITgcm, but no GM scheme for horizontal mixing. A detailed description of OCCAM is given by Marsh et al. (2005).

We have calculated the overturning streamfunctions using the time-dependent velocity and density fields simulated for the years 1987–2003. The overturning streamfunction as a function of density and depth is defined as

$$\psi(\rho, z) \equiv \frac{1}{t_1 - t_0} \int_{t_0}^{t_1} \iint_{S(\rho,z,t)} w \, dS \, dt, \tag{33}$$

where w is the vertical velocity, $dS = R\cos\phi d\phi d\lambda$ is a horizontal surface element, $S(\rho, z, t)$ is the area at depth z where the density is larger than ρ, t_0 is the beginning of 1987, and t_1 is the end of 2003. Note that the time integration is performed last, and not directly on the vertical velocity. This is essential, since the position of the isopycnals varies in time.

In accordance with the theoretical development in section 2, ρ in Eq. (33) is the in situ density. The resulting streamfunction is presented in Fig. 6a. We see that the circulation in the deep ocean is essentially confined to a narrow sloping band. The slope of this band is given by the adiabatic density change of a fluid parcel that moves vertically. By definition, the potential density is preserved during such adiabatic motion. Therefore, if we instead use potential density in Eq. (33), this band is vertical. Such a streamfunction is shown in Fig. 6b.

However, it should be remembered that adiabats are not uniquely defined in either of the figures, since parcels with different salinity have different adiabats. Correspondingly, the definition of potential density is not unique. In Fig. 6b we have used σ_2, but if we instead use σ_0 the streamfunction is slightly different. Therefore Fig. 6a is the correct one, although Fig. 6b gives a more visible picture. Also note that each of these two figures can be approximately obtained from the other one by a depth-dependent shift in the density direction, which leaves the area element $d\rho dp$ and therefore the thermodynamic work invariant.

The streamfunction in depth–density coordinates contains the three following distinct overturning cells.

1) In the shallowest 200 m, there is a clockwise cell that involves water lighter than approximately $\sigma = 26$. This is the blue cell to the left in Figs. 6a,b, with a volume transport of 62 Sverdrups (1 Sv $\equiv 10^6$ m^3 s^{-1}) and a conversion rate $C = 160$ GW from potential to kinetic energy. (C was calculated by numerical integration of ψ over the area in Fig. 6a where $\psi < 0$ and $\sigma < 28$.) It corresponds to the tropical cell in the World Ocean, where there is a wind-driven Ekman transport away from the equator. The poleward-flowing surface water is gradually

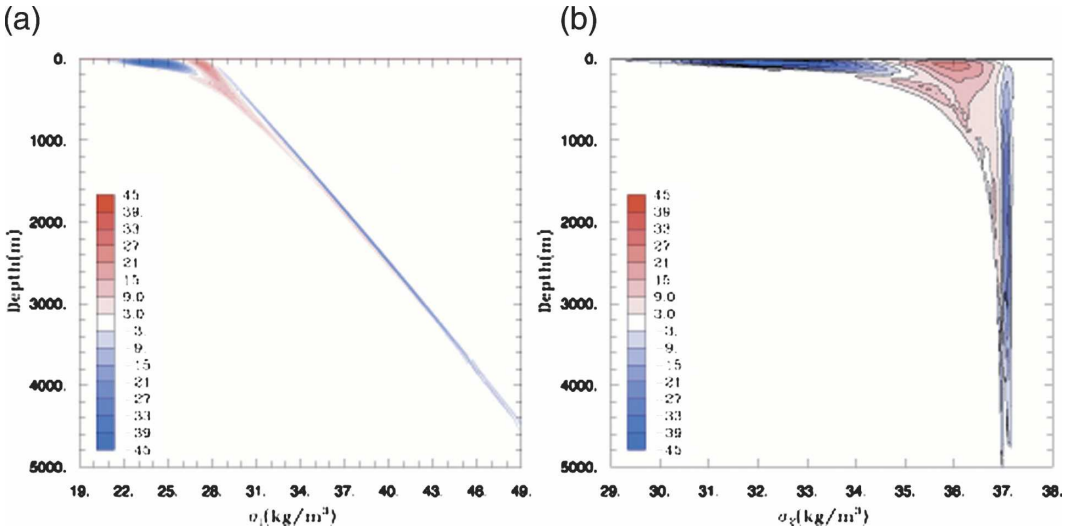

FIG. 6. Overturning streamfunction $\psi(\sigma, z)$ in depth–density coordinates from the OCCAM model (a) as a function of in situ density σ, and (b) as a function of potential density σ_2. The transport is given in Sverdrups and $\psi(\sigma, z)$ is counted positive (red shading) in anticlockwise cells and negative (blue shading) in clockwise cells.

cooled by heat loss to the atmosphere, until it is forced down into the subsurface layers by Ekman pumping. After downwelling approximately adiabatically to its maximum depth (at most a couple hundred meters), the water gradually rises back to the surface, while being heated by small-scale mixing. According to the sign of C, this cell should be classified as thermally forced (in reality forced by small-scale mixing). However, as illustrated by the box diagram in Fig. 2, C and T may be positive simultaneously, and it is likely that this cell is also forced by the Ekman transport. Thus, our interpretation is that the tropical overturning cell is forced both by the large scale wind stress and by the small-scale mixing.

2) The middle overturning cell is the anticlockwise red cell in Fig. 6. It stretches from the surface down to a depth of 2000 m, and mostly involves water heavier than $\sigma = 26$. The volume transport of this cell is 24 Sv, and it converts kinetic energy to potential energy at a rate of 140 GW. Thus, the conversion rate C is negative; that is, the sinking water is lighter than the rising water. A glance at Fig. 2 then reveals that the wind stress forcing T is the only possible source of kinetic energy, since the dissipation rate D is always positive. Thus, this cell can unambiguously be classified as mechanically forced by the large-scale Ekman pumping. We note that its sign is opposite to what would be expected from conventional assumptions about the deep circulation in the global ocean. This issue will be discussed in the following section.
3) To the right in Figs. 6a,b there is a very narrow and deep clockwise blue cell, only involving water with a density larger than 36.9 in σ_2 units. Its volume transport is 18 Sv, and it converts potential energy to kinetic energy at a rate of $C = 97$ GW. (C was calculated by numerical integration of ψ over the area in Fig. 6a where $\psi < 0$ and $\sigma > 28$.) Thus, the direction is thermally direct, implying that this cell is driven by the small-scale mixing that heats the water in the rising branch. Since it hardly touches the surface it seems unlikely that the wind stress plays a large role in forcing this cell, unlike the tropical cell.

In Table 2 we summarize the transports and conversion rates obtained for the three circulation cells. We also give the corresponding values obtained when using potential density (either σ_0 or σ_2) instead of in situ density as a coordinate. For the tropical cell almost the same values are obtained with all three methods. The conversion rates of the other two cells, however, depend significantly on the definition of density. (Remember that the correct values are obtained by using in situ density.) We conclude that the nonlinear nature of the equation of state plays an essential role for the energetics of the deep circulation.

We emphasize that particle trajectories do not follow the streamlines in Fig. 6, and that this streamfunction (like other overturning streamfunctions) is only a two-dimensional projection of an underlying complex three-dimensional flow field. Thus, each of the three cells mentioned above may be a superposition of several different circulations cells. It is also possible that there is a large overlap between the three cells that cancels

TABLE 2. Volume transport (Sv) and energy conversion C (GW) from potential energy to kinetic energy for the three overturning cells in OCCAM. The values have been calculated using both in situ density σ (the correct method) and potential density σ_0 and σ_2.

	Transport			C		
	σ	σ_0	σ_2	σ	σ_0	σ_2
Tropical cell	62	62	62	160	160	161
Middle cell	−24	−24	−24	−140	−111	−187
Deep cell	18	16	18	97	45	86

when they are superimposed, which would mean that the underlying three-dimensional circulation cells are stronger than they appear in Fig. 6a. Similar issues have recently been explored in a recent study of the overturning circulation in the Southern Ocean (Döös et al. 2005, manuscript submitted to *J. Geophys. Res.*).

For comparison, we also show the traditional overturning streamfunction as a function of latitude and depth in Fig. 7a, and the overturning streamfunction as a function of latitude and density in Fig. 7b, both calculated from the same OCCAM simulation as above. It is fairly straightforward to identify the tropical cell in all these plots, but apart from that it is far from obvious how the cells in the different streamfunctions correspond to each other. For example, what is the role of the Deacon Cell (the strong anticlockwise cell in the Southern Ocean in Fig. 7a) for the cells in Fig. 6? And where is the North Atlantic Deep Water in Fig. 6? In the future we intend to explore issues of this kind.

In Fig. 8 we show the horizontal integral of the streamfunction in depth–density coordinates, which gives the total vertical advective buoyancy flux as a function of depth [cf. Eq. (28)]. This flux is upward in the shallowest and deepest parts of the ocean, and downward in the intermediate range. Similar diagnostics were shown for a coarse-resolution global model in a study by Gnanadesikan et al. (2005). They found that the horizontally integrated advective buoyancy flux is everywhere directed downward, indicating that the flow is thermally indirect (i.e., mechanically forced). Apparently, the thermally direct tropical cell is absent or much weaker in their model than in OCCAM. A computation of the streamfunction in depth–density coordinates would reveal whether thermally direct cells at the lowest and highest densities exist in their model as well.

6. Discussion

As a background for the discussion, we first sketch the conventional picture of the basic dynamics of the global ocean circulation. According to this, the ocean is divided into two main regions: the thermocline, down to a depth of 500–1000 m, and the deep ocean. The dynamics in the thermocline is mainly adiabatic, and dominated by the wind stress via Ekman pumping. The dynamics in the deep ocean, on the other hand, is mainly advective–diffusive, with the primary balance in the buoyancy equation being between small-scale mixing and a very broad and slow upwelling. The deep water is resupplied by narrow convection events.

The division into two vertical regions can be justified by simple scaling arguments (Welander 1971; Whitehead 1995). The idea that the deep overturning circulation consists of a broad upwelling made possible by small-scale mixing on one hand, and narrow downward convection on the other hand, is the basis of essentially all theories of the deep circulation, starting with Stommel (1958) and Stommel and Arons (1960) (see also Pedlosky 1996). The assumed upwelling is too slow to be observed directly, but indirect estimates based on other oceanographic data have been made (Munk 1966; Munk and Wunsch 1998). There has been some discussion about whether this deep overturning circulation is

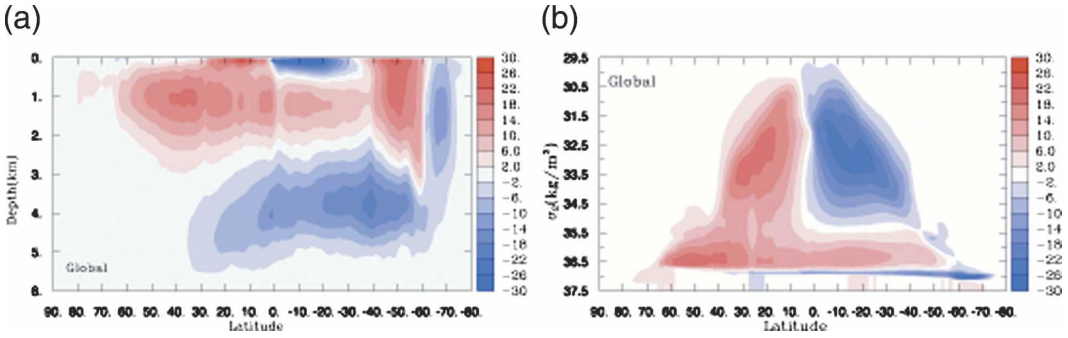

FIG. 7. Meridional overturning streamfunction from the OCCAM model (a) as a function of latitude and depth, and (b) as a function of latitude and potential density σ_2. The transport is given in Sverdrups and ψ is counted positive (red shading) in anticlockwise cells and negative (blue shading) in clockwise cells.

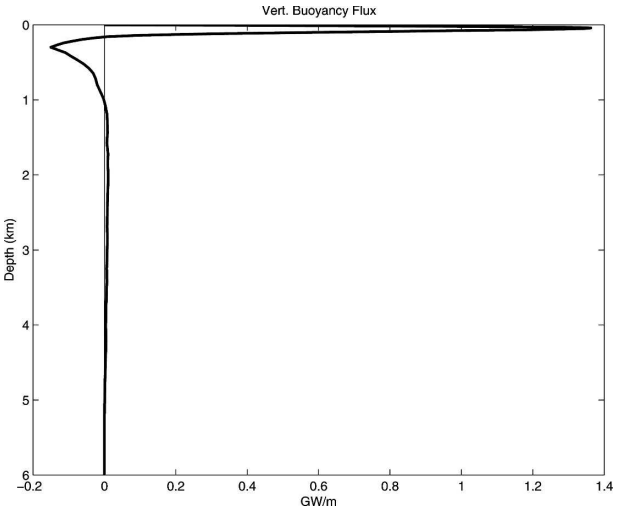

FIG. 8. Vertical advective buoyancy flux as a function of depth in the OCCAM model, obtained by integrating $-\psi$ in Fig. 6 along lines z = constant.

primarily forced by the upwelling or by the convection, and about whether it is mechanically or thermally forced, but its direction (i.e., that the cold water sinks and the warm water rises) has not been questioned.

Influenced by this conventional picture, we expected the following outcome of the idealized model experiments described in section 4. Without wind forcing, the whole circulation should be thermally direct. Adding the wind stress should result in an indirect cell in the thermocline, while a direct cell should remain in the deep ocean. However, the actual outcome was the opposite: the indirect, mechanically driven cell appeared in the deep ocean, while a direct cell remained in the warm surface layer, as seen in Fig. 4.

The streamfunction in depth–density coordinates for the realistic OCCAM model is remarkably similar to the one for the idealized model, as seen from Figs. 4 and 6. The main difference is the third, very narrow thermally direct cell in the densest water in Fig. 6. Only this cell seems to be compatible with the conventional picture of the deep circulation. Munk and Wunsch (1998) estimated that a power of around 400 GW from small-scale mixing is needed to force the deep circulation, while only 97 GW is needed by the deep cell in Fig. 6a. A part of this discrepancy might be explained by entrainment, which is not represented in the model. As a result of entrainment, the potential energy lost by convection is partly recovered by the associated vertical mixing. The importance of entrainment for the overturning circulation was recently emphasized by Hughes and Griffiths (2006).

At the same time, the overturning of waters lighter than 36.9 in σ_2 units down to a depth of more than 2000 m is dominated by the middle cell in Fig. 6, which is driven by the large-scale Ekman pumping. In this cell, the downwelling water is lighter than the upwelling water, and the main role of small-scale mixing is to cool this downwelling water, rather than to heat the upwelling water as in the circulation envisioned by Munk (1966), Munk and Wunsch (1998), and many others.

Thus, our thermodynamic analysis has revealed that the overturning circulation in the realistic high-resolution model OCCAM is rather different than the conventional picture of the real ocean. Note, however, that our analysis method singles out the diapycnal flow component, which is probably the least accurate aspect of numerical models, while filtering away the adiabatic component (along the isopycnal surfaces), for example, the large-scale gyre circulation. (The adiabatic component is much stronger and is better described by numerical models, and it has a strong influence on the overturning streamfunction in depth–latitude coordinates.) It would be interesting to apply our method to other models, for example an isopycnal model, which has a rather different treatment of the diapycnal flow than the z-coordinate model we have used.

Acknowledgments. We are grateful to Andrew Coward and the OCCAM team for the OCCAM data. We also thank Trevor McDougall for comments that have led to significant improvements of the paper.

REFERENCES

Andrews, D. G., and M. E. McIntyre, 1976: Planetary waves in horizontal and vertical shear: The generalized Eliassen–Palm relations and the mean zonal acceleration. *J. Atmos. Sci.,* **33,** 2031–2048.

Defant, A., 1961: *Physical Oceanography.* Vol. 1, Pergamon Press, 729 pp.

Döös, K., and D. J. Webb, 1994: The Deacon Cell and the other meridional cells in the Southern Ocean. *J. Phys. Oceanogr.,* **24,** 429–442.

Gade, H. G., and K. E. Gustafsson, 2004: Application of classical thermodynamic principles to the study of oceanic overturning circulation. *Tellus,* **56A,** 371–386.

Gnanadesikan, A., R. D. Slater, P. S. Swathi, and G. K. Vallis, 2005: The energetics of ocean heat transport. *J. Climate,* **18,** 2604–2616.

Huang, R. X., 1999: Mixing and energetics of the oceanic thermohaline circulation. *J. Phys. Oceanogr.,* **29,** 727–746.

Hughes, G. O., and R. W. Griffiths, 2006: A simple convective model of the global overturning circulation, including effects of entrainment into sinking regions. *Ocean Modell.,* **12,** 46–79.

Jeffreys, H. W., 1925: On fluid motions produced by differences of temperature and salinity. *Quart. J. Roy. Meteor. Soc.,* **51,** 347–356.

Karsten, R., H. Jones, and J. Marshall, 2002: The role of eddy transfer in setting the stratification and transport of a circumpolar current. *J. Phys. Oceanogr.,* **32,** 39–54.

Lichtenberg, A. J., and M. A. Lieberman, 1983: *Regular and Stochastic Motion.* Springer-Verlag, 499 pp.

Marchal, O., 2007: Particle transport in horizontal convection: Implications for the "Sandström theorem." *Tellus,* **59A,** 141–154.

Marsh, R., B. A. de Cuevas, A. C. Coward, H. L. Bryden, and M. Álvarez, 2005: Thermohaline circulation at three key sections in the North Atlantic over 1985–2002. *Geophys. Res. Lett.,* **32,** L10604, doi:10.1029/2004GL022281.

Marshall, J., A. Adcroft, C. Hill, L. Perleman, and C. Heisey, 1997a: A finite-volume, incompressible Navier–Stokes model for studies of the ocean on parallel computers. *J. Geophys. Res.,* **102** (C3), 5753–5766.

——, C. Hill, L. Perleman, and A. Adcroft, 1997b: Hydrostatic, quasi-hydrostatic, and non-hydrostatic ocean modeling. *J. Geophys. Res.,* **102** (C3), 5733–5752.

Mullarney, J. C., R. W. Griffiths, and G. O. Hughes, 2004: Convection driven by differential heating at a horizontal boundary. *J. Fluid Mech.,* **516,** 181–209.

Munk, W. H., 1966: Abyssal recipes. *Deep-Sea Res.,* **13,** 707–730.

——, and C. I. Wunsch, 1998: Abyssal recipes. II: Energetics of tidal and wind mixing. *Deep-Sea Res. I,* **45,** 1977–2010.

Nilsson, J., G. Broström, and G. Walin, 2005: Thermohaline circulation induced by bottom friction in sloping-boundary basins. *J. Mar. Res.,* **63,** 705–728.

Nurser, A. J. G., and M.-M. Lee, 2004a: Isopycnal averaging at constant height. Part I: The formulation and a case study. *J. Phys. Oceanogr.,* **34,** 2721–2739.

——, and ——, 2004b: Isopycnal averaging at constant height. Part II: Relating to the residual streamfunction in Eulerian space. *J. Phys. Oceanogr.,* **34,** 2740–2755.

Nycander, J., K. Döös, and A. C. Coward, 2002: Chaotic and regular trajecturies in the Antarctic Circumpolar Current. *Tellus,* **54A,** 99–106.

Paparella, F., and W. R. Young, 2002: Horizontal convection is non-turbulent. *J. Fluid Mech.,* **466,** 205–214.

Pedlosky, J., 1996: *Ocean Circulation Theory.* Springer, 453 pp.

Sandström, J. W., 1908: Dynamische Versuche mit Meerwasser. *Ann. Hydrodyn. Mar. Meteor.,* **36,** 6–23.

Stommel, H., 1958: The abyssal circulation. *Deep-Sea Res.,* **5,** 80–82.

——, and A. B. Arons, 1960: On the abyssal circulation of the world ocean. I. Stationary flow patterns on a sphere. *Deep-Sea Res.,* **6,** 140–154.

Welander, P., 1971: The thermocline problem. *Philos. Trans. Roy. Soc. London,* **270A,** 415–421.

Whitehead, J. A., 1995: Thermohaline ocean processes and models. *Annu. Rev. Fluid Mech.,* **27,** 89–113.

Wunsch, C., and R. Ferrari, 2004: Vertical mixing, energy, and the general circulation of the oceans. *Annu. Rev. Fluid Mech.,* **36,** 281–314.